Dentomaxillofacial Radiology (2020) 49, 20190202

birpublications.org/dmfr

RESEARCH ARTICLE

Head and neck osteosarcoma: CT and MR imaging features

[1,2]Zhendong Luo, [1]Weiguo Chen, [2]Xinping Shen, [1]Genggeng Qin, [3]Jianxiang Yuan, [4]Biying Hu, [2]Jianxun Lyu, [1]Chanjuan Wen and [1]Weimin Xu

[1]Department of Radiology, Nanfang Hospital, Southern Medical University, Guangzhou, China; [2]Department of Radiology, The University of Hong Kong - Shenzhen Hospital, Shenzhen, China; [3]Department of Radiology, Foshan traditional Chinese medicine Hospital, Foshan, China; [4]Department of Radiology, Foshan first people's Hospital, Foshan, China

Objective: This study aims to assess the CT and MRI features of head and neck osteosarcoma (HNO).
Methods: 37 HNOs were identified, and the following imaging characteristics were reviewed on CT and MRI.
Results: A total of 37 patients(age 41.5 ± 15.0 years old; 16 males, 21 females) were included in the study. Tumours occurred in the maxilla (16, 43.2%), mandible (8, 21.6%), skull base (6, 16.2%), calvarium (5, 13.5%), paranasal sinuses (1, 2.7%) and cervical soft tissue (1, 2.7%). 16 patients received radiotherapy for nasopharyngeal carcinoma. Three patients (8.1%) developed osteosarcomas related to a primary bone disease. 16 of the (43.2%) tumours demonstrated lytic density on CT scans, followed by 13 (35.1%) showing mixed density and 7 (18.9%) with sclerotic density. Matrix mineralization was present in 32 (86.5%). 3 out of 24 (12.5%) tumours showed lamellar periosteal reactions, 21 out of 24 (87.5%) showed spiculated periosteal reactions. 12 tumours showed low signal intensities on T_1WI, with 16 having heterogeneous signal intensities. 10 tumours showed high signal intensities on T_2WI, and 18 showed heterogeneous signal intensities. With contrast-enhanced images, 3 tumours showed homogeneous enhancement (2 osteoblastic and 1 giant cell-rich), 18 tumours showed heterogeneous enhancement (13 osteoblastic, 4 fibroblastic and 1 giant cell-rich), and 7 tumours showed peripheral enhancement (6 chondroblastic and 1 osteoblastic). These tumours were characterized by soft tissue masses with a diameter of 5.6 ± 1.8 cm.
Conclusions: HNO is a rare condition and is commonly associated with previous radiation exposure. This study provides age, sex distribution, location, CT and MRI features of HNO.
Dentomaxillofacial Radiology (2020) **49**, 20190202. doi: 10.1259/dmfr.20190202

Cite this article as: Luo Z, Chen W, Shen X, Qin G, Yuan J, Hu B, et al. Head and neck osteosarcoma: CT and MR imaging features. *Dentomaxillofac Radiol* 2020; **49**: 20190202.

Keywords: Osteosarcoma; Head; Neck; Computed tomography; Magnetic resonance imaging

Background

Osteosarcoma is the most common primary malignant bone tumour and mostly occurs in the metaphysis of long bones. Headand neck osteosarcoma (HNO) is a rare condition that accounts for less than 10% of all types of osteosarcoma and 1% or less of all head and neck cancers.[1,2] A small subset of patients present with a history of prior radiotherapy, and it is likely that osteosarcoma is induced by radiation in these individuals.[2] Patients with HNO have an average age of 45 and have a 20 year longer life expectancy than those with long bone osteosarcoma.[3–5] HNOs are often aggressive and have high histological grades.[4] Unlike tumours of the extremities, HNO presents a diagnostic challenge due to its rare occurrence, its variation in presenting complaints and its suboptimal visualization of the typical radiological features, which often leads to the misinterpretation of lesions as other diseases. Until now, there have been few studies reporting the imaging features of HNO,[6–10] with case reports only describing CT features in review articles and case series in the head and neck. The present large series aims to review the imaging features of HNO in CT and MRI scans from

Correspondence to: Weiguo Chen, E-mail: chenweiguo1964@21cn.com
Received 19 May 2019; revised 03 October 2019; accepted 15 October 2019

37 patients and to analyze the clinical and pathological characteristics of patients with HNO across three institutions from June 2005 to January 2019.

Methods

The study identified a total of 37 patients with HNO across 3 hospitals from all available electronic pathologic databases who met the inclusion criteria with a diagnosis of HNO based on open surgical resection (n = 15) and biopsy (n = 22). A trained radiologist with 12 years of experience reviewed the medical records to obtain demographic information on the patients' age and sex, history of prior radiation, latency of radiation-induced osteosarcoma and primary tumour site in which osteosarcoma could arise as a secondary lesion. A trained pathologist with 10 years of experience reviewed all available histological biopsies and/or resections and classified the tumours according to the World Health Organization histologic classification of bone tumours. Only patients with previously untreated, histologically confirmed HNO were included in this report. Tumour size was estimated through CT or MRI. CT examination was performed in all patients. A 16-slice CT scanner (LightSpeed Ultra 16, GE Healthcare, Milwaukee, WI) was used for 15 patients, and two 64-slice CT scanners (SOMATOM Definition AS, Siemens Healthcare, Erlangen, Germany) were used for 22 patients. The acquisition slice thickness was 3 mm, the sagittal and coronal reconstruction thickness was 5 mm with 5 mm intervals using bone or/and soft tissue algorithms. A 90 ml intravenous bolus dose of non-ionic iodinated contrast agent was administered at a rate of 3 $ml\,s^{-1}$. MR examination was performed in 28 patients. A 3.0 T MR imaging system (Signa Excite HD, GE Healthcare, Milwaukee, WI) was used in 21 patients, and a 1.5 T MR imaging system (Magnetom Avanto, Siemens Healthcare, Erlangen, Germany) was used in 7 patients. All images were obtained at a section thickness of 5 mm with a 1 mm intersection gap. Axial non-fat-suppressed T_2 weighted fast spin-echo [2100–4000/60–140 repetition time/echo time (TR/TE)], axial non-fat-suppressed T_1 weighted spin-echo [400–650/10–25 (TR/TE)] and axial gadolinium-enhanced fat-suppressed T_1 weighted spin-echo [460–630/9–25 (TR/TE)] images were obtained in all 28 patients.

The CT and MR imaging data were recorded for all patients. All baseline tumour imaging scans were obtained prior to treatment or intervention. All images were made available in real-time through the Picture Archiving and Communication System. The images were examined by two radiologists with more than 10 years of experience who were blinded to the tumour histological types. The analyses of CT imaging included (1) bone destruction (classified as lytic, osteoid, mixed, or none), (2) the presence of periosteal reaction (classified as none, lamellar or spiculated), (3) the presence of matrix mineralization (recorded as present or absent), (4) the margins of the mass (classified as ill- or well-defined) and (5) the size of the mass (based on MRI assessment or CT imaging by considering its longest diameter).

Analyses of MRIs were based on the (1) presence of a soft tissue component (recorded as present or absent), (2) size of the mass (measured using its longest diameter), and (3) signal intensities of the mass on T_2- and T_2 weighted images (classified as low, isointense, or high) compared with those of normal bone marrow and on contrast-enhanced images (classified as homogeneous, heterogeneous or with peripheral enhancement).

The diagnosis of osteosarcoma was established by clinical and imaging findings. It was confirmed on histologic slides of the tumor tissue specimens obtained from biospy, as well as by evaluation of the resected specimen. When the diagnosis of osteosarcoma was confirmed, the subtype was classified retrospectively using World Health Organization criteria.[11] This classification was made considering both biopsy and surgical specimens. The common feature in all cases was the presence of osteoid material or bone directly formed by undifferentiated tumor cells. On the basis of the predominant cell type and intercellular material (osteoid, cartilage, or collagen), osteosarcoma was classified as osteoblastic, fibroblastic, chondroblastic, giant cell-rich, small cell or well-differentiated variants.

Results

The clinical features of 37 patients with HNOs are summarized in Table 1. The study cohort comprised 37 patients with 16 males and 21 females, aged 41.5 ± 15.0 (range 9–68) years old. Tumours most frequently occurred in the maxilla (16 out of 37, 43.2%), followed by the mandible (8, 21.6%), skull base (6, 16.2%), calvarium (5, 13.5%), paranasal sinuses (1, 2.7%), and cervical soft tissue (1, 2.7%).

Among all patients, 16 patients (43.2%) received radiotherapy for nasopharyngeal carcinoma. One patient was diagnosed with radiation-induced extraskeletal osteosarcoma in the cervical soft tissue. Three patients (8.1%) developed osteosarcomas related to a primary bone disease, with two patients diagnosed with fibrous dysplasia and one with osteoblastoma.

Table 1 Clinical features of all 37 head and neck osteosarcomas

Location	*No.*	*%*	*M*	*F*	*Prior radiation*	*Underlying disease*
Maxilla	16	43.2	8	8	6	1
Mandible	8	21.6	4	4	2	1
Skull base	6	16.2	2	4	4	
Calvarium	5	13.5	1	4	2	1
Paranasal sinuses	1	2.7	1	0	1	0
Cervical soft tissue	1	2.7	0	1	1	0
Total	37	100	16	21	16	3

Table 2 The histology of all 34 high-grade head and neck osteosarcomas

Histological subtypes	*Primary*	*Radiation-induced osteosarcoma*	*Total*
Osteoblastic	7	12	19
Chondroblastic	7	1	8
Fibroblastic	2	3	5
Giant cell-rich	2	0	2
Total	18	16	34

In terms of the histological classification, most (34, 91.8%) tumours consisted of high-grade HNO, with the histology summarized in Table 2. The histological subtype was reported as conventional high-grade in almost (32, 94.1%) all cases; more than half (19, 59.4%) were reported as osteoblastic, followed by a quarter (8, 25%) that were reported as chondroblastic, fibroblastic (5, 15.6%), and giant cell-rich tumours (2, 5.9%).

The clinical and histological subtypes of 16 cases of radiation-induced HNOs are illustrated in Table 3. The median latency period from the end of radiation therapy to the diagnosis of radiation-induced osteosarcoma was 9.7 years (range 2.5–20 years). More than half of the cases of radiation-induced osteosarcoma (9, 56.3%) occurred 5–10 years after radiotherapy, and up to 87.5% of the cases of radiation-induced osteosarcoma developed within 15 years after radiotherapy. All the cases were considered primary tumours at the initial evaluation.

Imaging evaluations of the tumours at the time of presentation included CT (37, 100%) and MRI (28, 75.7%). More than 80% of patients (30, 81.1%) underwent contrast-enhanced CT, while all patients received contrast-enhanced MRI.

Table 4 summarizes the CT imaging features of HNOs. One patient was shown to have extraskeletal osteosarcoma without bone destruction (Figure 1), whereas most patients (36, 97.3%) had varying degrees of bone destruction (Figures 2–5); none of the patients had pathological fractures. 16 patients were shown to have lytic density (Figure 3), with 13 of mixed density (Figures 2 and 4) and 7 of sclerotic density (Figure 5). More than 85% (32, 86.5%) of the patients had soft tissue masses that penetrated into cortical bone with invasion of the surrounding soft tissue. Almost all (6, 97.3%) tumours were heterogeneous in attenuation. The majority (32, 86.5%) of tumours exhibited matrix mineralization (Figures 1–5). Periosteal reactions were observed in 24 patients, the majority (21, 87.5%) of which were spiculated periosteal reactions (Figures 2 and 4); the remaining patients included those with (3, 12.5%) and without (13, 35.1%) lamellar periosteal reactions.

The MRI features of HNO in 27 patients are summarized in Table 5. 12 patients (42.9%) showed low signal intensities on T_1 weighted images, with 16 (57.1%) showing heterogeneous signal intensities in muscle (Figures 2–5). 10 (35.7%) patients showed high signal intensities on T_2 weighted images, with 18 (64.3%) showing heterogeneous signal intensities (Figures 2–5).

Table 6 summarizes the relationships between the various enhancement patterns of MRI images and the histological subtypes of 28 HNOs. Contrast-enhanced scanning was performed in all patients. On contrast-enhanced images, 18 tumours showed heterogeneous enhancement [osteoblastic (13, 72.2%), fibroblastic (4, 22.2%) and (1, 5.6%) giant cell-rich] (Figures 2, 3 and 5), whereas 3 demonstrated homogeneous enhancement (two were osteoblastic, and the other was giant cell-rich), with the remaining tumours showing peripheral

Table 3 The clinical and histological subtypes of 16 radiation-induced head and neck osteosarcomas

Case no.	*Histological subtypes*	*Location*	*Age (years)*	*Latency (years)*	*Size*	*Metastasis at the initial evaluation*
1	Osteoblastic	Paranasal sinuses	48	9	5.6	No
2	Chondroblastic	Cervical soft tissue	40	6	2.5	No
3	Osteoblastic	Temporal bone	53	10	3.9	No
4	Osteoblastic	Temporal bone	40	8	8.0	No
5	Fibroblastic	Sphenoid bone	62	9	6.3	No
6	Osteoblastic	Sphenoid bone	50	12	7.4	No
7	Osteoblastic	Sphenoid bone	19	2.5	7.1	No
8	Osteoblastic	Sphenoid bone	57	14	4.8	No
9	Osteoblastic	Maxilla	62	6	8.0	No
10	Fibroblastic	Maxilla	41	8	7.1	No
11	Osteoblastic	Maxilla	26	5	8.2	No
12	Osteoblastic	Maxilla	56	17	3.1	No
13	Osteoblastic	Maxilla	57	15	2.3	No
14	Osteoblastic	Mandible	41	7	3.5	No
15	Fibroblastic	Mandible	51	20	4.9	No
16	Osteoblastic	Mandible	50	5	2.4	No

Table 4 The CT imaging characteristics of all 37 head and neck osteosarcomas

Location	*Bone destruction*				*Matrix mineralization*		*Periosteal reaction*		*Margin definition*		
	Mixed	*Lytic*	*Osteoid*	*No*	*Yes*	*No*	*Spiculated*	*Lamellar*	*No*	*Ill*	*Well*
Maxilla	6	7	3	0	13	3	9	1	6	13	3
Mandible	2	3	3	0	8	0	5	1	2	6	2
Skull base	2	4	0	0	5	1	3	0	3	0	6
Calvarium	3	2	0	0	4	1	3	1	1	1	4
Paranasal sinuses	0	0	1	0	1	0	1	0	0	0	1
Cervical soft tissue	0	0	0	1	1	0	0	0	1	0	1
Total	13	16	7	1	32	5	21	3	13	20	17

enhancement of chondroblastic (6, 85.7%) (Figure 4) and osteoblastic (1, 14.3%) subtypes. The mean mass size was measured on CT or MR as approximately 5.6 ± 1.8 cm (range, 2.4–10.0 cm; median, 5.4 cm).

Discussion

Osteosarcoma is the most common malignant bone tumour that affects long bones in children and adolescents with HNO and is known to be a rare condition. A limited number of studies have described the occurrence of HNO among different small-sized patient population groups. In the present study, HNO arose in a number of sites with the most common occurrence in the craniofacial region, specifically in the maxilla.[1] Our study results were in accordance with those of a literature review, whereby it was common for skull osteosarcoma to be present in the middle of the skull base.[12] In our study, a patient was diagnosed with radiation-induced extraskeletal osteosarcoma with a tumour located in the cervical soft tissue. Extraskeletal osteosarcoma is a rare malignancy that is different from conventional osteosarcoma of bone in terms of both clinical and radiological perspectives. Roller et al[13] reported that most of these tumours occurred in extremities, with one in the neck, of which the patient had a history of previous radiotherapy at the site of the tumour.

With more than a third of patients (43.2%) presenting with a history of prior radiotherapy, and all the primary tumours in our study were nasopharyngeal carcinoma. Three patients within the study developed osteosarcoma related to a primary bone disease (fibrous dysplasia and osteoblastoma), which was in agreement with other studies.[2,14,15]

According to our results, the mean age of HNO patients ranges from 26 to 40 years old, which is in line with the literature.[16–18] In our series, lesions in 37 patients occurred over a wide age range (9–68 years old), with a mean age of 41.5 years old. HNO tends to develop in females, with a male-to-female ratio of 1:1.31, as shown in our study. This male-to-female ratio was similar to that of the one stated in a review article reported by Chen et al with a ratio of 1:1.21.[16]

More than 90% of patients in the current study had high-grade tumours, with the majority of tumours classified as osteoblastic rather than chondroblastic

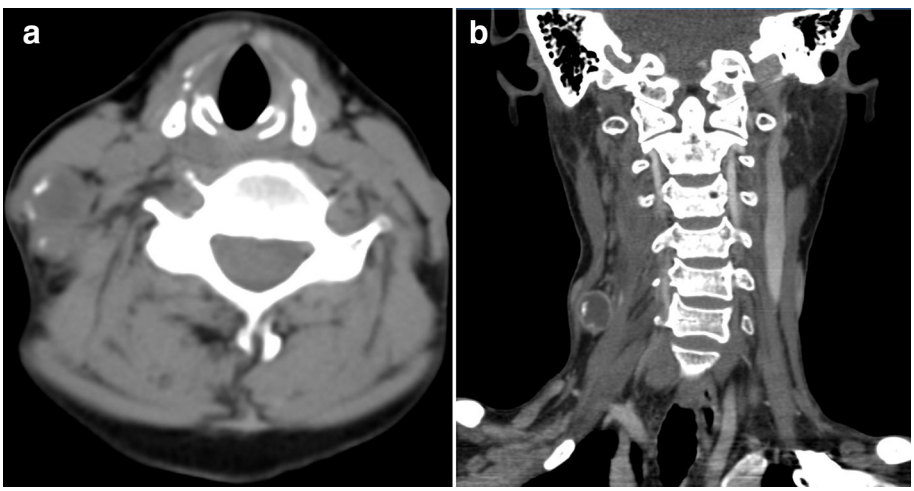

Figure 1 (a, b) A 40-year-old female with radiation-induced extraskeletal osteosarcomas in cervical soft tissue 5 years after nasopharyngeal carcinoma radiotherapy (histological subtypes, chondroblastic). (a) Axial CT with the soft tissue algorithm showing a soft tissue mass posterior to the right sternocleidomastoid and separate from the cervical vertebra with hyperdense peripheral matrix mineralization (white arrows). (b) Post-contrast multiplanar reformatted coronal CT scan with the soft tissue algorithm showing a peripheral rim-enhancing soft tissue mass.

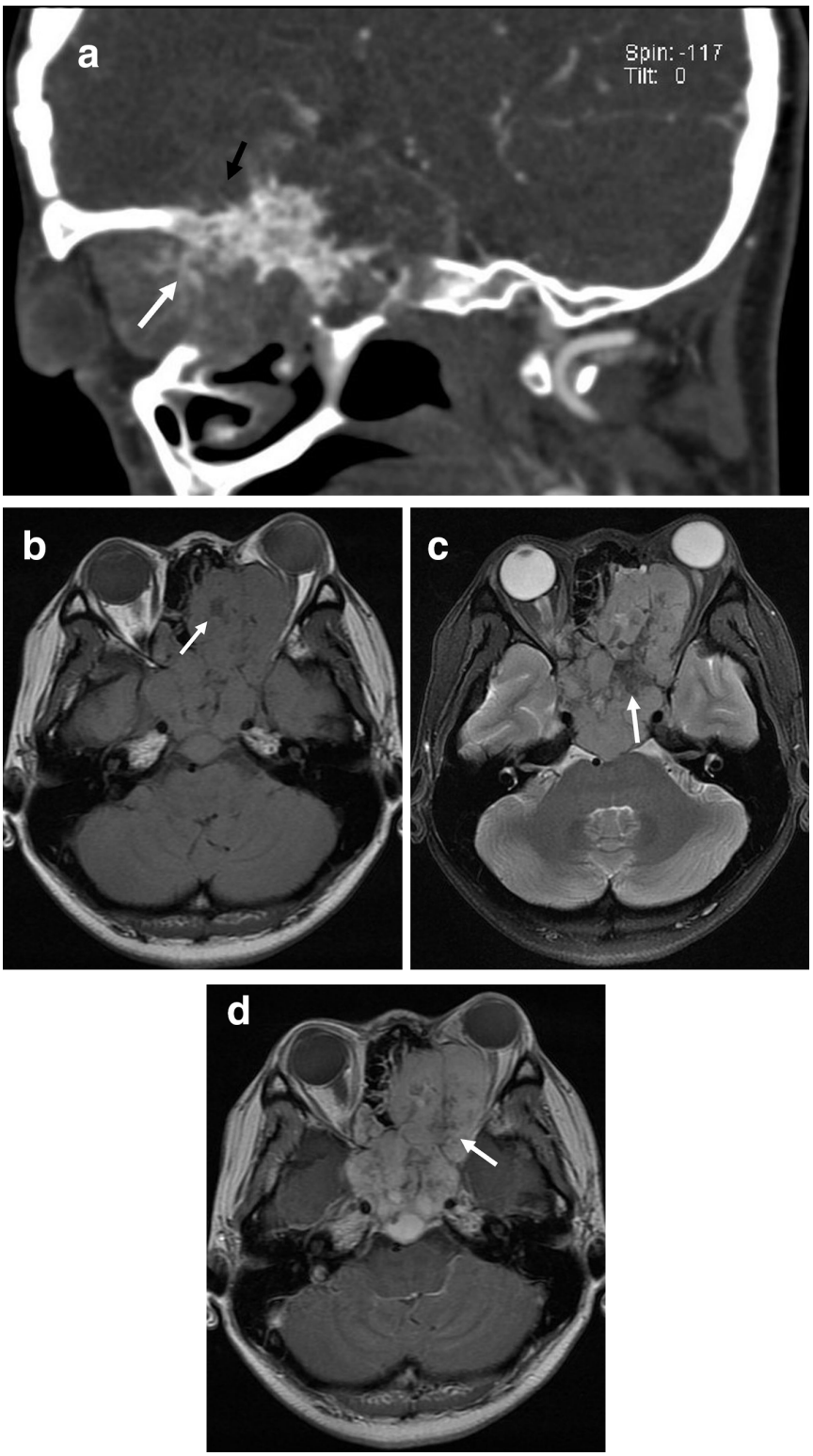

Figure 2 (a–d) A 33-year-old female with osteosarcoma of the middle skull base (histological subtypes, osteoblastic). (a) Multiplanar reformatted sagittal CT with the bone algorithm showing mixed lytic and blastic lesions of sphenoidalis, suggestive of matrix mineralization (white arrows) and spiculated periosteal reactions (black arrows). (b) Axial T_1 weighted image of the soft tissue component showing heterogeneous signal intensity with patchy low signal intensities, suggestive of matrix mineralization (white arrows). (c) FLAIR image of the soft tissue component showing heterogeneous high signal intensity with patchy low signal intensities, suggestive of matrix mineralization (white arrow). (d) Axial T_1 weighted contrast-enhanced image showing a heterogeneous markedly enhancing mass in the sphenoid sinus with low signal intensity, suggesting matrix mineralization (white arrow) with lesions extending into the ethmoid sinus and right orbit. FLAIR,fluid-attenuated inversion recovery.

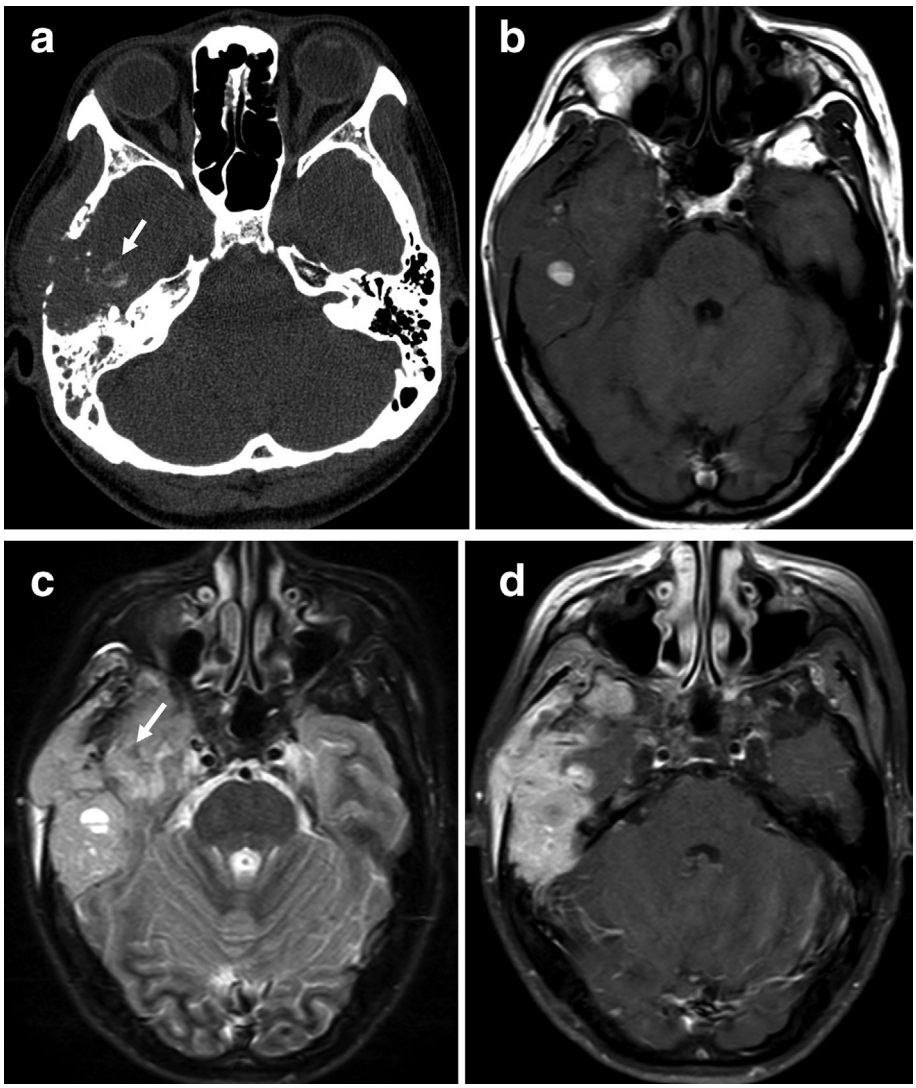

Figure 3 (a–d) A 40-year-old female with osteosarcoma of the right temporal bone (histological subtypes, osteoblastic). (a) Axial CT with the bone algorithm showing a lytic lesion of the right temporal bone with extraosseous soft tissue extension, suggestive of matrix mineralisation (white arrows). (b) Axial T_1 weighted image of the soft tissue component showing heterogeneous signal intensity with patchy high signal intensity, suggestive of haemorrhage (white arrows). (c) FLAIR image of the soft tissue component showing heterogeneous high signal intensity with patchy low signal intensity, suggestive of matrix mineralization (white arrow). (d) Axial T_1 weighted contrast-enhanced image showing a heterogeneous markedly enhancing mass in the right temporal bone with a lesion invading the temporal lobe.

and fibroblastic, which is consistent with the results of previous studies.[4,5,19] Surprisingly, although most of the patients in the current study had high-grade osteoblastic tumours, the most common types of primary osteosarcoma were chondroblastic and osteoblastic.

CT and MRI both have their own superiorities in detecting osteosarcoma, and the combination of CT and MRI indeed improved the diagnostic accuracy for patients suffering from osteosarcoma.[20] The osteosarcomas in the present series had CT features similar to those of osteosarcoma of the extremities.[6,21] HNO primarily exhibits osteolysis and/or osteoblastic destruction, as well as having an irregular tumour margin on CT imaging. The mixed and sclerotic radiological pattern in the head and neck region is highly suggestive of osteosarcoma, with differential diagnoses of metastasis, lymphoma, and chondrosarcoma. The primary features are local or patchy high-density shadows in the medullary cavity with varying degrees of bone destruction and matrix mineralization. All lesions were of considerable size when first observed, and osteoid-type calcification was demonstrated in almost all patients. The characteristic osteoid matrix production of HNO is of high density on unenhanced CT scans. The pattern of periosteal reaction can be classified as aggressive or non-aggressive according to Rana et al.[22] Aggressive reactions include laminated, spiculated (hair-on-end, sunburst), disorganized, or Codman triangle reaction patterns, while non-aggressive periosteal reactions include thin, solid, thickly irregular, or septated

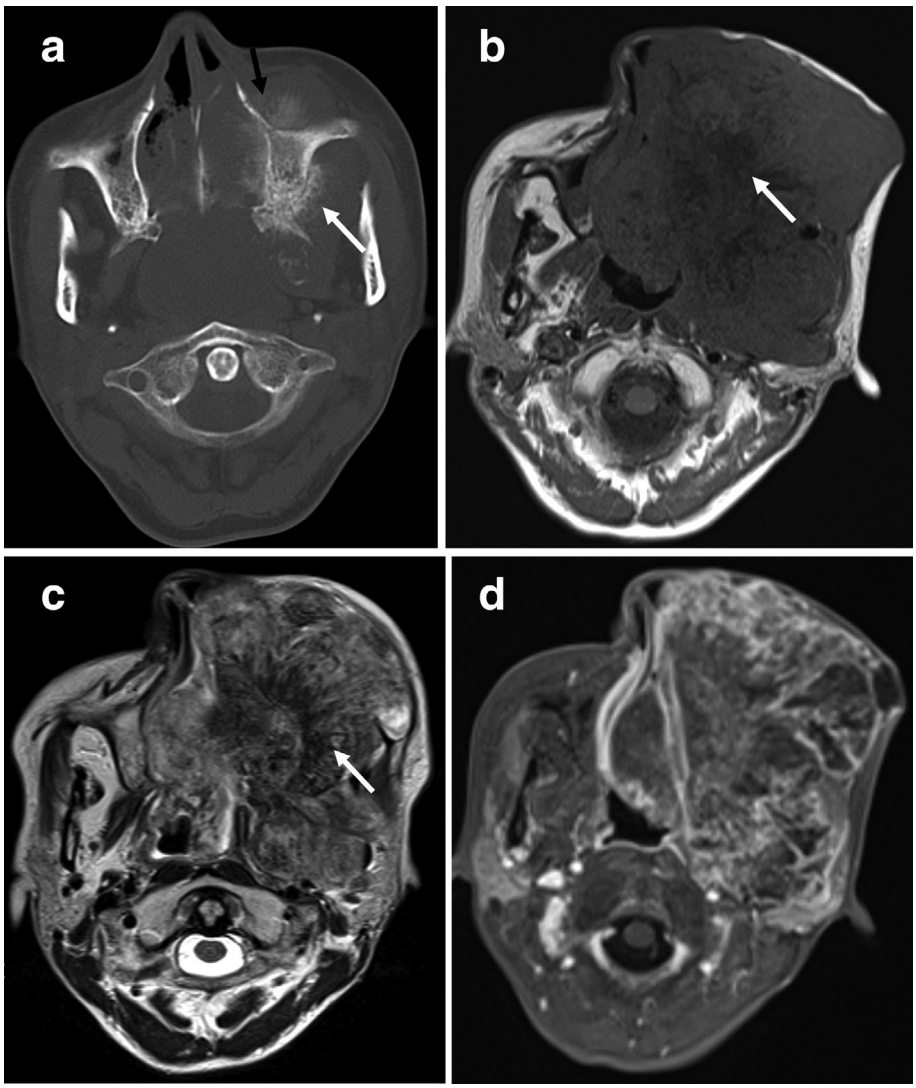

Figure 4(a–d) A 43-year-old female with osteosarcoma of the left maxilla (histological subtypes, chondroblastic). (a) Axial CT with the bone algorithm showing a mixed lytic and blastic lesion of the left maxilla with large extraosseous soft tissue extension, suggestive of matrix mineralization (white arrows) and spiculated periosteal reactions (black arrows). (b) MRI performed 3 months after the CT examination. Axial T_1 weighted image showing an increase in tumour size with the soft tissue component showing heterogeneous signal intensity and patchy low signal intensity, suggestive of matrix mineralization (white arrow). (c) Axial T_2 weighted image of the soft tissue component showing heterogeneous high signal intensity with patchy low signal intensity, suggestive of matrix mineralization (white arrow). (d) Fat-suppressed axial T_1 weighted contrast-enhanced image showing a peripheral rim-enhancing soft tissue mass.

patterns. The speculated (sunburst, hair-on-end) or Codman triangle subtypes of periosteal reactions are most frequently observed in bones of the extremities. In our study, cases of HNOs with a spiculated periosteal reaction were common (56.8%), but those with a lamellar periosteal reaction were rare (8.1%). Bone destruction without periosteal reaction also existed in some cases of HNO. These results are similar to those of Wang et al,[6] who found the presence of periosteal reactions of any kind in 62% of patients, and he speculated that periosteal reactions were more common than laminated reactions.

MRI is widely accepted as the imaging method of choice for the evaluation of the extent of primary lesions and their relationship with anatomic structures. MRI depicts soft tissues and bone marrow infiltration (medulla) better than CT imaging, showing cortical destruction and expansive masses. The masses within this study showed low (n = 12) or heterogeneous signal intensities (n = 16) on T_1 weighted images and high (n = 10) or heterogeneous signal intensities (n = 18) on T_2 weighted images. These masses can contain haemorrhage or necrosis as well as osteoid matrix, which are both commonly found in osteosarcoma.[23] The importance of non-enhanced and Gd-DTPA-enhanced MR imaging has been demonstrated by their ability to enhance tissue characterization in some instances with heterogeneous or peripheral enhancements related to

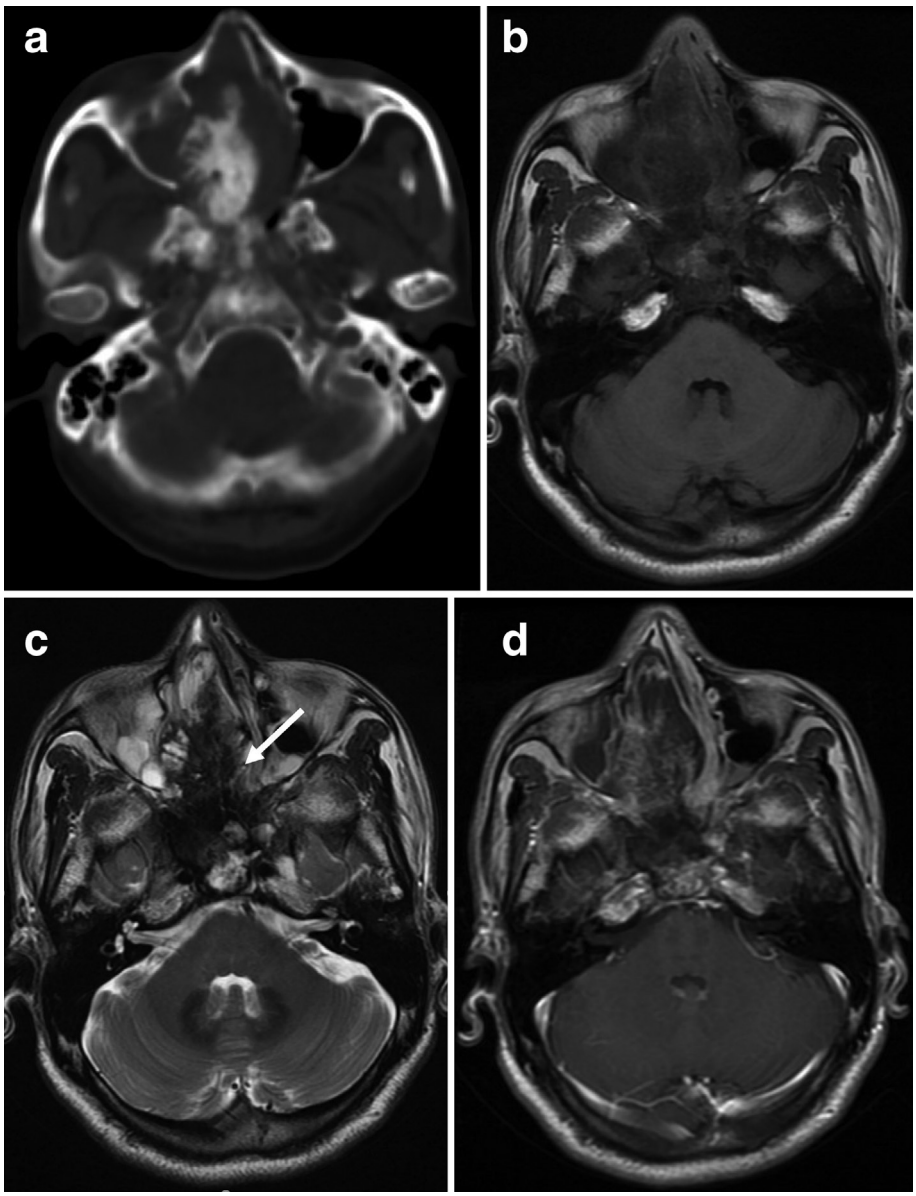

Figure 5 (a–d.) A 48-year-old male with osteosarcoma of the right paranasal sinuses 9 years after radiotherapy for nasopharyngeal carcinoma (histological subtypes, osteoblastic). (a) Axial CT with the bone algorithm showing the tumour mass with osteoblastic destruction of the right paranasal sinuses. (b) Axial T_1 weighted image of the soft tissue component showing low signal intensity. (c) Axial T_2 weighted image of the soft tissue component showing heterogeneous high signal intensity with agglomerate low signal intensity, suggestive of matrix mineralization (white arrow). (d) Axial T_1 weighted contrast-enhanced image showing a heterogeneously enhancing mass in the right paranasal sinuses.

various components (osteoid matrix, haemorrhage, and necrosis) within tumour masses.[24] MRI plays an important role in depicting the tumour location and size. However, despite recent improvements in MRI techniques,[25] the histological diagnosis of bone tumours by MRI remains challenging. In our study, although the features of osteoblastic osteosarcoma on MRI scans were non-specific and rather indistinguishable from the features of other sarcomas with T2 hyperintense signals and heterogeneous post-contrast enhancement, peripheral rim enhancement was observed on Gd-enhanced MR imaging, which supports the diagnosis of chondroblastic osteosarcoma.

The early diagnosis and treatment of HNO are of great importance, and the diagnosis of HNOs should be considered when individuals exhibit previously described symptoms or imaging characteristics.

Several limitations exist in our study. First, although the number of patients was relatively large, the number of several histological subtypes remained limited, which could be explained by the rare occurrence of osteosarcoma occurring within the head and neck region.

Table 5 The MRI characteristics of 28 head and neck osteosarcomas

Location	*Soft tissue component*		T_1*WI*		T_2*WI*		*Magnetic resonance contrast- enhancement patterns*		
	Present	*Absent*	*Low*	*Heterogeneous*	*High*	*Heterogeneous*	*Heterogeneous*	*Homogeneous*	*Peripheral*
Maxilla	9	1	5	5	3	7	9	0	1
Mandible	6	0	1	5	1	5	2	1	2
Skull base	6	0	3	3	3	3	2	1	3
Calvarium	5	0	2	3	3	2	1	1	3
Paranasal sinuses	1	0	1	0	0	1	1	0	0
Total	27	1	12	16	10	18	15	3	10

T_1 WI, T_1 weighted imaging; T_2WI, T_2 weighted imaging.

Table 6 The various enhancement patterns of magnetic resonance images correlated with histological subtypes of 28 head and neck osteosarcomas

Histological subtypes	*Magnetic resonance contrast enhancement—patterns*			
	Heterogeneous	*Homogeneous*	*Peripheral*	*Total*
Osteoblastic	13	2	1	16
Chondroblastic	0	0	6	6
Fibroblastic	4	0	0	4
Giant cell-rich	1	1	0	2
Total	18	3	7	28

Second, different CT or MR scanners and protocols were used, and not all the patients had both CT and MR examinations performed. This technical difficulty could be avoided since data were collected from three different hospitals. Third, the present series focused on the CT and MR imaging features of HNO, and no treatment strategies or clinical outcomes were documented, with a number of patients lost to follow-up. Finally, this was a retrospective study. Nevertheless, a prospective study would be rather difficult to conduct because it is uncommon for osteosarcoma to occur in the head and neck region.

Conclusions

HNO is rare, and for those cases that do develop, they are often associated with previous radiation exposure. The features of osteoblastic HNO on MRI scans are non-specific and often indistinguishable from those of other types of sarcoma with T2 hyperintense signals and heterogeneous post-contrast enhancement. Nevertheless, the peripheral rim enhancement observed on Gd-enhanced MR images supports the diagnosis of chondroblastic HNO. An initial diagnosis of HNO should be considered when tumours with matrix mineralization are present early in the fourth decade of life. In lieu of these unusual locations and challenges in differentiating osteosarcomas from other common tumours, keeping these clinical and imaging features in mind will support the diagnosis with a high degree of confidence.

Acknowledgment

This study was supported by High Level-Hospital Program, Health Commission of Guangdong Province, China (NO: 201901026).

References

1. Huber GF, Dziegielewski P, Wayne Matthews T, Dort JC. Head and neck osteosarcoma in adults: the province of Alberta experience over 26 years. *J Otolaryngology Head Neck Surg* 2008; **37**: 738–43.
2. Mendenhall WM, Fernandes R, Werning JW, Vaysberg M, Malyapa RS, Mendenhall NP. Head and neck osteosarcoma. *Am J Otolaryngol* 2011; **32**: 597–600. doi: https://doi.org/10.1016/j.amjoto.2010.09.002
3. Xie Y, Zhang Z, Hong J, Liu W, Lu H, Du Y, et al. Furazolidone-containing triple and quadruple eradication therapy for initial treatment for Helicobacter pylori infection: a multicenter randomized controlled trial in China. *Helicobacter* 2018; **23**: e12496. doi: https://doi.org/10.1111/hel.12496
4. Liang L, Zhang T, You Y, He Q, Fan Y, Liao G. An individual patient data meta-analysis on the effect of chemotherapy on survival in patients with craniofacial osteosarcoma. *Head Neck* 2019; **41**: 2016–23. doi: https://doi.org/10.1002/hed.25668
5. Chen Y, Gokavarapu S, Shen Q, Liu F, Cao W, Ling Y, et al. Chemotherapy in head and neck osteosarcoma: adjuvant chemotherapy improves overall survival. *Oral Oncol* 2017; **73**: 124–31. doi: https://doi.org/10.1016/j.oraloncology.2017.08.017
6. Wang S, Shi H, Yu Q. Osteosarcoma of the jaws: demographic and CT imaging features. *Dentomaxillofac Radiol* 2012; **41**: 37–42. doi: https://doi.org/10.1259/dmfr/86834844

7. Long M-yun, Diao F-yu, Peng L-na, Tan L-ping, Zhu Y, Huang K, et al. Effect of neurological monitoring in postoperative 5-15 days residual thyroidectomy after primary thyroid cancer surgery. *Asia Pac J Clin Oncol* 2018; **14**: e332–5. doi: https://doi.org/10.1111/ajco.12981
8. Shi Y, Liu MX, Long XL, Chen DJ, Zheng HY, Chen SL. Effect of abnormal GpG methylation in the second trimester of pregnancy on adverse health risk of offspring. *Exp Ther Med* 2018; **16**: 2875–80.
9. Bianchi SD BA, Gandini G. Radiologic features of osteosarcoma of the jaw. *La Radiol Med* 1995; **89**: 586–92.
10. Shibuya HKT, Iwaki H, Ohashi I, Yamada I, Suzuki S. Ct findings in primary osteosarcoma of the jaw. *RoFo* 1991; **154**: 139–42.
11. Fletcher CDM, Bridge JA, Hogendoorn PCW, Mertens F editores. *World Health Organization classification of tumours of soft tissue and bone*. IARC: Lyon; 2013.
12. Guo Z, Hu K, Zhao B, Bian E, Ni S, Wan J. Osteosarcoma of the skull base: an analysis of 19 cases and literature review. *Journal of Clinical Neuroscience* 2017; **44**: 133–42. doi: https://doi.org/10.1016/j.jocn.2017.06.014
13. Roller LA, Chebib I, Bredella MA, Chang CY, Clinical CCY. Clinical, radiological, and pathological features of extraskeletal osteosarcoma. *Skeletal Radiol* 2018; **47**: 1213–20. doi: https://doi.org/10.1007/s00256-018-2908-6
14. Reis C, Genden EM, Bederson JB, Som PM. A rare spontaneous osteosarcoma of the calvarium in a patient with long-standing fibrous dysplasia: CT and Mr findings. *Br J Radiol* 2008; **81**: e31–4. doi: https://doi.org/10.1259/bjr/19620568
15. Pack SE, Al Share AA, Quereshy FA, Baur DA. Osteosarcoma of the mandible arising in fibrous Dysplasia—A case report. *Journal of Oral and Maxillofacial Surgery* 2016; **74**: 2229.e1–2229.e4. doi: https://doi.org/10.1016/j.joms.2016.06.174
16. Chen Y, Shen Q, Gokavarapu S, Lin C, YahiyaC, Cao W, et al. Osteosarcoma of head and neck: a retrospective study on prognostic factors from a single Institute database. *Oral Oncol* 2016; **58**: 1–7. doi: https://doi.org/10.1016/j.oraloncology.2016.04.008
17. Liang J, Meng W-D, Yang J-M, Li S-L, Zhong M-N, Hou X-X, et al. The association between liver cirrhosis and fracture risk: a systematic review and meta-analysis. *Clin Endocrinol* 2018; **89**: 408–13. doi: https://doi.org/10.1111/cen.13762
18. Kassir RR, Rassekh CH, Kinsella JB, Segas J, Carrau RL, Hokanson JA. Osteosarcoma of the head and neck: meta-analysis of nonrandomized studies. *Laryngoscope* 1997; **107**: 56–61. doi: https://doi.org/10.1097/00005537-199701000-00013
19. PK H, Eisele DW, Frassica FJ, Zahurak ML, McCarthy EF. Osteosarcoma of the head and neck: a review of the Johns Hopkins experience. *Laryngoscope* 1999; **109**: 964–9.
20. Zhao S, Zeng D, Song J, Liang J, Zhou Y, Zhu Y, et al. Comparative analysis of diagnostic value between magnetic resonance imaging and computed tomography for patients with osteosarcoma. *j med imaging hlth inform* 2018; **8**: 295–8. doi: https://doi.org/10.1166/jmihi.2018.2339
21. Gangadhar K, Santhosh D. Primary skull osteosarcoma: MDCT evaluation and histopathological correlation in two cases. *Neuroradiol J* 2012; **25**: 188–92. doi: https://doi.org/10.1177/197140091202500206
22. Rana RS, Wu JS, Eisenberg RL. Periosteal reaction. *American Journal of Roentgenology* 2009; **193**: W259–72. doi: https://doi.org/10.2214/AJR.09.3300
23. Murphey MD, Robbin MR, McRae GA, Flemming DJ, Temple HT, Kransdorf MJ. The many faces of osteosarcoma. *RadioGraphics* 1997; **17**: 1205–31. doi: https://doi.org/10.1148/radiographics.17.5.9308111
24. Parry MC, Laitinen M, Albergo J, Jeys L, Carter S, Gaston CL, et al. Osteosarcoma of the pelvis. *Bone Joint J* 2016; **98-B**: 555–63. doi: https://doi.org/10.1302/0301-620X.98B4.36583
25. Erlemann R, Reiser MF, Peters PE, Vasallo P, Nommensen B, Kusnierz-Glaz CR, Ritter J, et al. Musculoskeletal neoplasms: static and dynamic Gd-DTPA--enhanced MR imaging. *Radiology* 1989; **171**: 767–73. doi: https://doi.org/10.1148/radiology.171.3.2717749